Mendeleev Communications

Mendeleev Commun., 2027, **37**, in press

Polymetallic catalysts based on high-entropy alloys $FeCoNiCuCrMAl_x$ (M = Mn, Re, La, Ce) for CO_2 hydrogenation

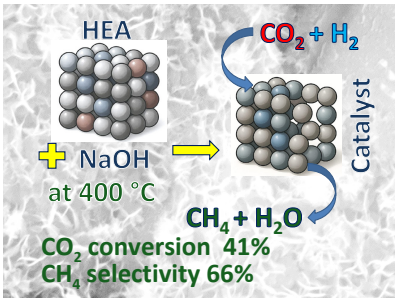
Elena V. Pugacheva,*[a] Ksenia A. Romazeva,[a] Evgenia I. Knerelman[b] and Vyacheslav N. Borshch[a]

[a] *A. G. Merzhanov Institute of Structural Macrokinetics and Materials Science, Russian Academy of Sciences, 142432 Chernogolovka, Moscow Region, Russian Federation. E-mail: help@ism.ac.ru*

[b] *Federal Research Center of Problems of Chemical Physics and Medicinal Chemistry, Russian Academy of Sciences, 142432 Chernogolovka, Moscow Region, Russian Federation*

DOI: 10.71267/mencom.8173

Polymetallic catalysts were fabricated by leaching high-entropy high-aluminum alloys $FeCoNiCuCrMAl_x$ (M = Mn, Re, La, Ce) synthesized *via* combined centrifugal casting–self-propagating high-temperature synthesis and were tested in CO_2 hydrogenation reaction. Ce and Mn modifiers enhanced catalytic activity at low temperatures, while Re and La inhibited performance. Unmodified FeCoNiCuCr catalyst was found to demonstrate the highest efficiency at 400 °C, achieving 41% conversion with a methane selectivity of 66%.



Keywords: self-propagating high-temperature synthesis, high-entropy alloys, polymetallic catalysts, CO_2 hydrogenation, methane.

Recently, interest in heterogeneous catalysts based on multicomponent (⩾ 5) transition metal alloys in near-equiatomic concentrations, known as high-entropy alloys (HEAs), has increased exponentially. Their unique properties, such as lattice distortion, slow diffusion and multi-element synergy, provide enhanced structural stability and tunable catalytic performance. HEAs are most widely employed as catalysts in electrochemical processes,[1–4] including electrocatalytic energy conversion technology.[2] In these processes, HEAs of various compositions exhibit activity in both reduction[5–8] and oxidation[9–11] reactions. Furthermore, HEAs also show promise in propane dehydrogenation[12] and CO_2 hydrogenation.[13–15] The latter is a key environmental strategy for reducing greenhouse gases and synthesizing value-added hydrocarbons.

Catalytic applications necessitate novel approaches to the synthesis of high-entropy materials. Established methods, such as argon-arc melting, mechanical alloying[16] and self-propagating high-temperature synthesis (SHS),[16,17] have been well-studied and enable the preparation of chemically homogeneous bulk alloys. However, the resulting monolithic materials possess a relatively low specific surface area, which is a critical parameter for active catalysts. The review[18] summarized various techniques for synthesizing nanoscale HEA particles, including carbon thermal shock, microwave synthesis, laser ablation, *etc*. Among these, selective chemical etching,[3,4,6,10] which involves removal of one alloy component, is particularly noteworthy. The resulting porous material exhibits a hierarchical pore structure and high specific surface area, which is highly beneficial for catalyst performance.

This paper presents a method for producing nanostructured catalytic materials using high-aluminum 3d-transition metal HEA precursors synthesized *via* combined centrifugal casting–SHS process.[15,19] To achieve a high specific surface area, aluminum is removed using concentrated alkali solutions.[20,21] This approach enables the preservation of the original HEA crystal structure without losing the active 3d-metal components.

We prepared several HEA precursors $FeCoNiCuCrMAl_x$, where M = Mn, Re, La, Ce with 50 wt% (for details, see Online Supplementary Materials). All catalysts were evaluated for CO_2 hydrogenation at atmospheric pressure. This reaction served as a primary assessment of catalytic activity prior to testing the samples under high-pressure conditions for the production of heavier hydrocarbons. Most of the metals comprising the investigated HEAs were previously evaluated by us in this process[21] in various binary and ternary combinations, while some modifiers were sourced from the literature.[14] Notably, the base core of the composition (Fe, Co, Ni) is frequently reported in the literature as a component of CO_2 hydrogenation catalysts. We also observed good reproducibility of the HEA structure in the synthesis of both precursors[19] and catalysts.

XRD patterns of catalysts (Figure 1) exhibit reflections corresponding to two iron-based solid solutions: one with a BCC lattice (*1*) (PDF2 card 010-73-8033) and another with a simple cubic lattice (*2*) (PDF2 card 85-1410), consistent with the phases identified in the precursor alloys.[19] After leaching, the catalysts retain their HEA structure. The precursor also contains an aluminide phase (*3*), which disappears during leaching (see Figure 1). Crystallite sizes were calculated using the Scherrer equation from the main reflection at 57° (Table 1). The reflections of the two phases overlap, so these results cannot be assigned to a single phase. Additionally, the proximity of the two lines causes substantial peak broadening, which results in the underestimated crystallite sizes.

The samples were characterized by low-temperature nitrogen adsorption method. Their specific surface areas and weight loss values are presented in Table 1. The nitrogen adsorption/desorption isotherms of catalysts (Figure S1) correspond to type IV according to the IUPAC classification, which is characteristic

© 2027 Mendeleev Communications

Table 1 Textural characteristics of samples and weight loss during leaching.[a]

Entry	Sample	D/ Å	S_{BET}/ $m^2\ g^{-1}$	V_p/ $cm^3\ g^{-1}$	R_p/ Å	V_{mic}/ $cm^3\ g^{-1}$	S_{mic}/ $m^2\ g^{-1}$	S_{mes}/ $m^2\ g^{-1}$	Weight loss (%)
1	FeCoNiCuCr	9	18	0.019	21	0.0061	11	7	15.6
2	FeCoNiCuCrRe	18	9	0.012	27	0.0031	5	4	7.7
3	FeCoNiCuCrMn	11	7	0.007	20	0.0024	6	1	5.2
4	FeCoNiCuCrLa	16	10	0.009	18	0.0037	8	2	8.9
5	FeCoNiCuCrCe	31	14	0.010	13	0.0058	13	2	8.7

[a] D is average crystallite size calculated using the Scherrer equation. S_{BET} is BET surface area. V_p is pore volume. R_p is pore radius. V_{mic} is micropore volume. S_{mic} is micropore surface area. S_{mes} is mesopore surface area.

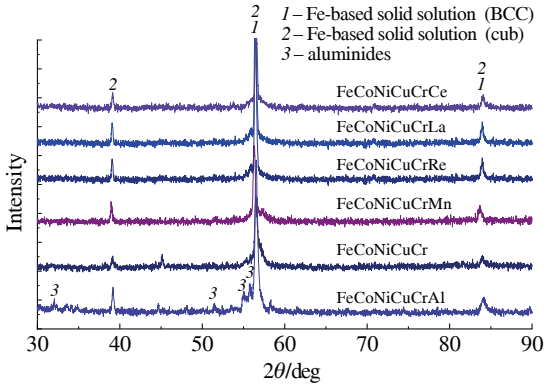


Figure 1 XRD patterns of catalysts: (*1*) Fe-based solid solution (BCC); (*2*) Fe-based solid solution (cube); (*3*) aluminides.

of mesoporous materials. The presence of mesopores is further confirmed by pore size distribution curves (Figure S1). The hysteresis loop shape assumes the presence of slit-like pores or plane-parallel particles, alongside a minor fraction of micropores.

The nominal compositions of precursors were designed in such a way that after aluminum removal, the Fe, Co, Ni, Cu and Cr ratios would remain near-equiatomic, with Mn, Re, La and Ce modifiers at 5 wt%. As can be seen from SEM/EDS results (Figures S2–S6, Tables S1–S5), FeCoNiCuCrMn and FeCoNiCuCrRe samples align with nominal values. In contrast, Ce and La surface concentrations are lower than expected because of the non-uniform distribution in the initial HEA precursors, which is explained in ref. 19. Despite their low content, these elements significantly influence catalytic activity. Catalysts contain some residual aluminum which is confirmed by weight loss data (Table 1) and SEM/EDS analysis (see Figures S2–S6, Tables S1–S5). Aluminum is effectively removed only from regions with its high concentration (on the order of 50 wt%). Phases with low Al content (Mal_2, MAl and lower) are highly corrosion-resistant in alkaline media. This results in the variation in aluminum concentrations across the surface. The significant scatter in the concentrations of the base metals can be explained by their varying solubility in aluminum and in each other, which is already evident in the micrographs of the precursor samples.[19] In our experience, the loss of base metals during the leaching stage is negligible; however, minor losses of metals that form oxyanions (Cr, Mn) are possible during the stabilization stage with H_2O_2 solution. Iron is the most uniformly distributed element on the surface (Tables S1–S5), which is consistent with XRD data indicating the presence of two iron-based solid solution phases in the sample compositions. The presence of a significant amount of oxygen on the surface (averaging 10.5–24 wt%) raises questions. The surface oxygen content varies several-fold from point to point (Tables S1–S5), often falling below the values calculated even for lower oxides. Apparently, part of the surface may be covered by a layer of oxides or hydroxides, while another part may be covered by adsorbed oxygen.

During the leaching process, a network of deep cracks forms on the surface, while exhibiting significant morphological heterogeneities. Whereas some surface areas remain relatively smooth, others develop a nanostructure consisting of plates or flakes oriented perpendicular to the surface and interconnected. The characteristic sizes of these structures vary significantly depending on the catalyst composition (Figure 3, Figures S2–S6).

Figure 3 shows the test results. The main reaction products were CH_4, H_2O and CO. Differences in the activity of catalysts with various additives are particularly pronounced in the low-temperature region and at 400 °C. For catalysts with Mn and Ce modifiers, CO_2 conversion initiates above 200 °C, reaching approximately 10% at 250 °C. For samples containing Re and La, significant conversion begins above 300 °C. FeCoNiCuCrRe catalyst shows maximum conversion at 350 °C, while the peak CO_2 conversion for the remaining catalysts is attained at 400 °C. Conversion values at 350 °C are comparable for all samples except FeCoNiCuCrRe. Three-fold repetition of the experiment for FeCoNiCuCrLa, as a representative sample of the group with similar conversion at 350 °C (Figure S8), showed that we could not confidently differentiate the conversion levels of samples *1*, *2*, *4* and *5* at 350 °C. In contrast, at 400 °C, the selection of the most active samples (FeCoNiCuCr, followed by FeCoNiCuCrLa) is quite reliable. FeCoNiCuCr sample exhibits the highest methane selectivity across the entire investigated temperature range. Selectivity is highly temperature-dependent, with all catalysts showing a maximum at 350 °C, followed by a decline in favor of CO production. A peculiarity of these catalysts is that CO is formed not only at elevated temperatures, but also at sufficiently low temperatures. A reduction in the hydrogen

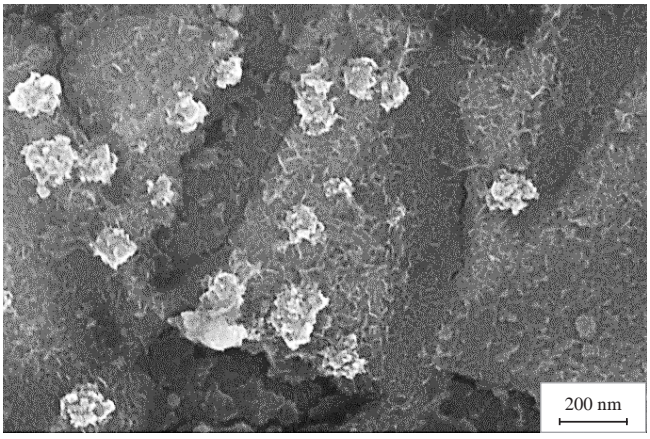


Figure 2 SEM micrograph of FeCoNiCuCr catalyst surface.

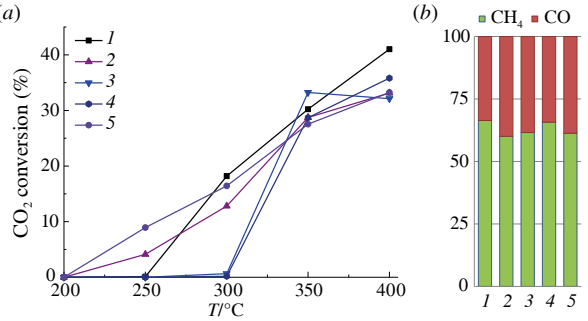


Figure 3 (*a*) Conversion of CO_2 and (*b*) selectivity at 400 °C in hydrogenation process over catalysts: *1* – FeCoNiCuCr, *2* – FeCoNiCuCrMn, *3* – FeCoNiCuCrRe, *4* – FeCoNiCuCrLa, *5* – FeCoNiCuCrCe. $CO_2 : H_2 = 1 : 4$, GHSV = 3600 h^{-1}.

content of the gas mixture causes a decrease in conversion, shifting the process toward CO formation (Figure S9–S10).

As shown in Table 1 and Figure 3, there is no direct correlation between structural/textural parameters and catalyst activity, except for the most active FeCoNiCuCr sample, which exhibits the smallest crystallite size and the highest specific surface area. Surface morphology also shows no direct correlation (see Figures S2–S6 and Figure 3). We believe that directly linking these parameters for catalysts with varying chemical compositions is inappropriate. It has been shown that even minor, impurity-level amounts of La and Ce modifiers strongly affect the surface distribution of other elements, particularly Ni, which is most active in hydrogenation (Tables S1–S5). It appears that the distribution of elements, and thus of active sites, is more critical than other parameters; however, establishing a direct link to the activity of specific samples is currently challenging.

Catalyst stability test results revealed that the FeCoNiCuCrMn and FeCoNiCuCrRe remain active for 1.5–4 h, while FeCoNiCuCrLa and FeCoNiCuCrCe show a ~5% drop in conversion after 1.5 h (Figure S11). The most active sample displays irregular behavior with a tendency toward decreasing activity, a phenomenon previously described in the literature.[14]

A comparison of our results with literature data showed that even noble metal catalysts on high-surface-area supports demonstrate comparable or worse activity and CH_4 selectivity (Table S6). Similarly, supported nickel-based catalysts with significantly higher surface areas do not consistently outperform others, inasmuch as this depends on the support and the deposition method. This also holds true for complex oxide catalysts. We also considered supported HEA catalysts, which demonstrated comparable results. It should be noted that data on their specific surface area are unavailable; furthermore, one of the samples contains Ru and Pd, whereas the other operates at a temperature of 700 °C and yields CO only.

In conclusion, high-aluminum FeCoNiCuCrMAl_x (M = Mn, Re, La and Ce) HEA were successfully prepared *via* combined centrifugal casting–SHS process and used as precursors for polymetallic catalysts. Following the removal of excess aluminum, the resulting catalysts exhibited a significantly increased specific surface area, while maintaining the HEA lattice structure, as confirmed by XRD analysis. Structural studies revealed that the catalyst granules were primarily characterized by slit-like mesopores and plane-parallel particles, supplemented by a substantial fraction of micropores. The catalysts were tested in CO_2 hydrogenation to methane at atmospheric pressure and demonstrated high activity. Ce and Mn modifiers enhanced the low-temperature activity of samples, whereas Re and La dopants reduced it. All additives except La reduce methane selectivity. The La-containing sample exhibits methane selectivity similar to that of FeCoNiCuCr. The maximum conversion and methane selectivity at 400 °C, 41% and 66%, respectively, were achieved on FeCoNiCuCr sample.

This work was performed in accordance with the State Assignment FFS2-2025-0002, state registration no. 125021201985-8 and the State Assignment FFSG-2024-0016, state registration no. 124020500064-2 using the equipment of the Center for Collective Use 'New Petrochemical Processes, Polymer Composites, and Adhesives' of FRC PCP and MC RAS (no. 77601) and the ISMAN Center of Shared Services. Special thanks are extended to A. O. Sivakova for assistance in interpreting the SEM/EDS results and N. Yu. Khomenko for assistance in interpreting the XRD results.

Online supplementary materials

Supplementary data associated with this article can be found in the online version at doi: 10.71267/mencom.8173.

References

1 Y. Zhou, X. Shen, M. Wang, L. Zhang, T. Qian, C. Yan and J. Lu, *Sci. China Mater.*, 2023, **66**, 2527; https://doi.org/10.1007/s40843-022-2436-6.
2 J. Chen, L. Ren, X. Chen, Q. Wang, C. Chen, J. Fan, S. Wang, V. Binas and S. Shen, *Exploration*, 2025, **5**, 20230036; https://doi.org/10.1002/EXP.20230036.
3 S. Li, J. Wang, X. Lin, G. Xie, Y. Huang, X. Liu and H.-J. Qiu, *Adv. Funct. Mater.*, 2021, **31**, 2007129; https://doi.org/10.1002/adfm.202007129.
4 G. Fang, J. Gao, J. Lv, H. Jia, H. Li, W. Liu, G. Xie, Z. Chen, Y. Huang, Q. Yuan, X. Liu, X. Lin, S. Sun and H.-J. Qui, *Appl. Catal., B*, 2020, **268**, 118431; https://doi.org/10.1016/j.apcatb.2019.118431.
5 Q. Zhang, S. Zhang, Y. Luo, Q. Liu, J. Luo, P.K. Chu and X. Liu, *APL Mater.*, 2022, **10**, 070701; https://doi.org/10.1063/5.0097479.
6 S. Li, X. Tang, H. Jia, H. Li, G. Xie, X. Liu, X. Lin and H.-J. Qiu, *J. Catal.*, 2020, **383**, 164; https://doi.org/10.1016/j.jcat.2020.01.024.
7 S. Nellaiappan, N. K. Katiyar, R. Kumar, A. Parui, K. D. Malviya, K. G. Pradeep, A. K. Singh, S. Sharma, C. S. Tiwary and K. Biswas, *ACS Catal.*, 2020, **10**, 3658; https://doi.org/10.1021/acscatal.9b04302.
8 J. Choi, H. Lim, G. H. Jeong and U. Sim, *Meet. Abstr.*, 2024, **MA2024-02**, 2141; https://doi.org/10.1149/MA2024-02282141mtgabs.
9 H. Luo, L. Li, F. Lin, Q. Zhang, K. Wang, D. Wang, L. Gu, M. Luo, F. Lv and S. Guo, *Adv. Mater.*, 2024, **36**, 2403674; https://doi.org/10.1002/adma.202403674.
10 X. Chen, C. Si, Y. Gao, J. Frenzel, J. Sun, G. Eggeler and Z. Zhang, *J. Power Sources*, 2015, **273**, 324; https://doi.org/10.1016/j.jpowsour.2014.09.076.
11 N. Zhang, X. Chen, S. Liu, J. Meng, M. Armbrüster and C. Liang, *ACS Appl. Mater. Interfaces*, 2023, **15**, 23276; https://doi.org/10.1021/acsami.3c02810.
12 J. Luo, X. Li, Y. Ye, T. Zhou, W. Wu, H. Li, Q. Yang, H. Yan and J. Zeng, *Angew. Chem., Int. Ed.*, 2025, **64**, e202419093; https://doi.org/10.1002/anie.202419093.
13 K. Mori, N. Hashimoto, N. Kamiuchi, H. Yoshida, H. Kobayashi and H. Yamashita, *Nat. Commun.*, 2021, **12**, 3884; https://doi.org/10.1038/s41467-021-24228-z.
14 C. Su, L. Wang, S. Zou, X. Zhang, H. Sun, X. Liu, C. Li, Y. Jiang, X. Li, J. Li and J. Huang, *Mater. Today Sustain.*, 2024, **28**, 101006; https://doi.org/10.1016/j.mtsust.2024.101006.
15 E. V. Pugacheva, S. Ya. Zhuk, I. M. Bystrova, K. A. Romazeva, D. M. Ikornikov, O. D. Boyarchenko, N. Yu. Khomenko, O. V. Belousova, V. N. Sanin and V. N. Borshch, *Int. J. Self-Propag. High-Temp. Synth.*, 2024, **33**, 200; https://doi.org/10.3103/S1061386224700158.
16 A. S. Rogachev, *Phys. Met. Metallogr.*, 2020, **121**, 733; https://doi.org/10.1134/S0031918X20080098.
17 V. N. Sanin, D. M. Ikornikov, A. O. Sivakova, D. Yu. Kovalev and O. A. Golosova, *Int. J. Self-Propag. High-Temp. Synth.*, 2024, **33**, 308; https://doi.org/10.3103/S1061386224700298.
18 H. Ali, Y. Xu, X. Han and Y. Lin, *Adv. Sci.*, 2025, e14577; https://doi.org/10.1002/advs.202514577.
19 E. Pugacheva, D. Ikornikov, A. Sivakova, K. Romazeva, D. Andreev, O. Golosova, V. Borshch and V. Sanin, *Metals*, 2025, **15**, 1381; https://doi.org/10.3390/met15121381.
20 V. N. Borshch, S. Ya. Zhuk, E. V. Pugacheva, Ts. D. Dipheko, D. E. Andreev, Yu. A. Agafonov and O. L. Eliseev, *Mendeleev Commun.*, 2023, **33**, 55; https://doi.org/10.1016/j.mencom.2023.01.017.
21 V. N. Borshch, E. V. Pugacheva, S. Ya. Zhuk, E. M. Smirnova, N. R. Demikhova and V. A. Vinokurov, *Russ. Chem. Bull.*, 2020, **69**, 1697; https://doi.org/10.1007/s11172-020-2950-0.

Received: 14th August 2026; Com. 26/8173

Mendeleev Commun., 2027, **37**, in press

Contents entry

Polymetallic catalysts based on high-entropy alloys $FeCoNiCuCrMAl_x$ (M = Mn, Re, La, Ce) for CO_2 hydrogenation

Elena V. Pugacheva, Ksenia A. Romazeva,
Evgenia I. Knerelman, Vyacheslav N. Borshch

